

muon $g - 2$ and the B -physics anomalies in RPV supersymmetry and the discovery prospect at LHC and future colliders

Fang Xu

Collaborators: Bhupal Dev, Amarjit Soni

Pheno 2021

Washington University in St. Louis

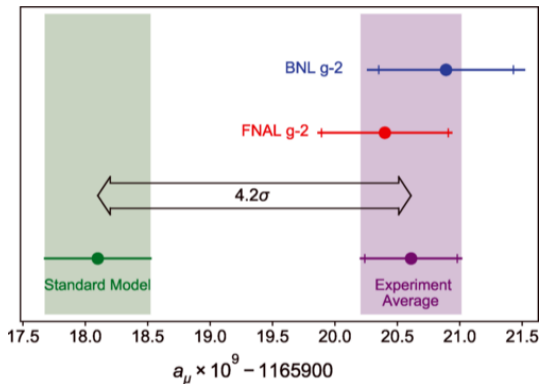
May 25, 2021

Motivation

- The recent experimental results of muon $g - 2$ (from the Fermilab) and the lepton flavor universality violation in rare B-meson decays (from the LHCb etc.) could be the hints of new physics beyond the Standard Model.
- Under the minimal RPV supersymmetric framework, assuming the mass of third generation sfermions lighter than the other two generations (called "RPV3", [Altmannshofer, Dev, Soni \(PRD 2017\)](#))
- muon $g - 2$ and the B -physics anomalies could be addressed simultaneously and also could be detected at LHC and beyond.

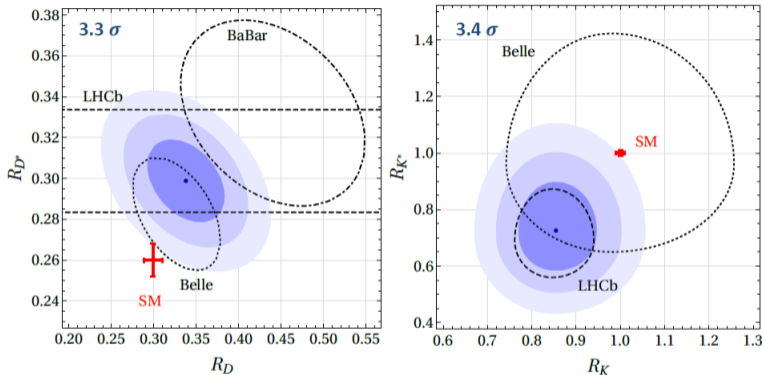
muon $g - 2$ anomaly

- $\Delta a_\mu = a_\mu^{\text{exp}} - a_\mu^{\text{SM}} = (251 \pm 59) \times 10^{-11}$ has a significance of 4.2σ .
- Could be the signal of new physics beyond the SM where some new couplings to muon could be detectable by LHC or future colliders.



B. Abi et al. (PRL 2021)

B-physics anomalies



Altmannshofer, Dev, Soni, Sui (PRD 2020)

- $R_{D^{(*)}} = \frac{\text{BR}(B \rightarrow D^{(*)} \tau \nu)}{\text{BR}(B \rightarrow D^{(*)} \ell \nu)}$ (with $\ell = e, \mu$), $R_{K^{(*)}} = \frac{\text{BR}(B \rightarrow K^{(*)} \mu^+ \mu^-)}{\text{BR}(B \rightarrow K^{(*)} e^+ e^-)}$
- Also imply the possible new couplings to leptons.

Explanation of anomalies in RPV3 SUSY

- The LQD and LLE part of the RPV SUSY Lagrangian which contains the λ' and λ couplings respectively and are relevant for the $R_{D^{(*)}}$, $R_{K^{(*)}}$ and $(g-2)_\mu$ anomalies.

$$\begin{aligned} \mathcal{L}_{LQD} = & \lambda'_{ijk} (\tilde{\nu}_{iL} \bar{d}_{kR} d_{jL} + \tilde{d}_{jL} \bar{d}_{kR} \nu_{iL} + \tilde{d}_{kR}^* \bar{\nu}_{iL}^c d_{jL} \\ & - \tilde{e}_{iL} \bar{d}_{kR} u_{jL} - \tilde{u}_{jL} \bar{d}_{kR} e_{iL} - \tilde{d}_{kR}^* \bar{e}_{iL}^c u_{jL}) + \text{H.c.} \end{aligned} \quad (1)$$

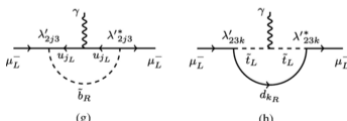
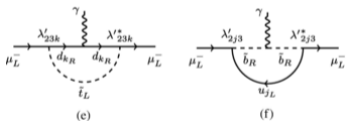
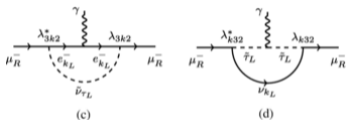
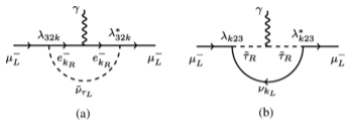
$$\mathcal{L}_{LLE} = \frac{1}{2} \lambda_{ijk} [\tilde{\nu}_{iL} \bar{e}_{kR} e_{jL} + \tilde{e}_{jL} \bar{e}_{kR} \nu_{iL} + \tilde{e}_{kR}^* \bar{\nu}_{iL}^c e_{jL} - (i \leftrightarrow j)] + \text{H.c.} \quad (2)$$

- Following previous discussions ([Kim, Kyaee, Lee \(PLB 2001\)](#); [Altmannshofer, Dev, Soni, Sui \(PRD 2020\)](#)), in RPV3 framework, $(g-2)_\mu$ correction can be written as:

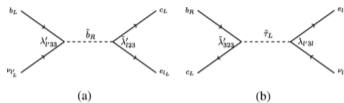
$$\Delta a_\mu = \frac{m_\mu^2}{96\pi^2} \sum_{k=1}^3 \left(\frac{2(|\lambda_{32k}|^2 + |\lambda_{3k2}|^2)}{m_{\tilde{\nu}_\tau}^2} - \frac{|\lambda_{3k2}|^2}{m_{\tilde{\tau}_L}^2} - \frac{|\lambda_{k23}|^2}{m_{\tilde{\tau}_R}^2} + \frac{3|\lambda'_{2k3}|^2}{m_{\tilde{b}_R}^2} \right) \quad (3)$$

Explanation of anomalies in RPV3 SUSY

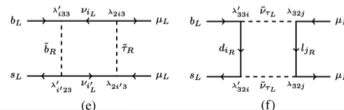
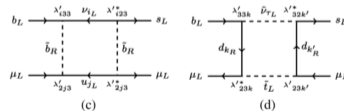
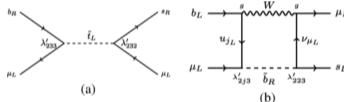
$(g - 2)_\mu$ Kim, Kyaee, Lee (PLB 2001)



$R_{D^{(*)}}$ Deshpande, He (EPJC 2017); Altmannshofer, Dev, Soni (PRD 2017) etc.



$R_{K^{(*)}}$ Das, Hati, Kumar, Mahajan (PRD 2017); Trifinopoulos (EPJC 2018) etc.



Parameters and benchmark scenario

- Parameters $(\lambda_{232}, \lambda'_{233}, \lambda'_{223}, \lambda'_{232}, m_{\tilde{b}_R}, m_{\tilde{b}_L}, m_{\tilde{\nu}_\tau}, m_{\tilde{\tau}_L})$
 - $\lambda_{232} = -\lambda_{322} \neq 0 \Leftrightarrow$ contribute to muon $g - 2$, other λ_{3ij} couplings cannot be large at the same time due to the constraints of $\tau \rightarrow \mu\mu\mu$, $\tau \rightarrow e\mu\mu$ etc.
 - $\lambda'_{2ij} \neq 0 \Leftrightarrow$ include μ and free of $m_{\tilde{\nu}_\tau}$, otherwise, λ'_{3ij} combined with λ_{32k} or λ_{3k2} , well measured meson decays $(\bar{d}_i d_j) \rightarrow \mu\ell_k$ or $\tau \rightarrow \mu K$ and $\tau \rightarrow \mu\eta$ decays will prevent λ'_{3ij} to be large.
 - $m_{\tilde{\tau}_R}$ not involved with this choice of couplings.
 - $m_{\tilde{t}_L}$ can only influence $\text{BR}(B_s \rightarrow \mu^+ \mu^-)$ and the Wilson coefficients $(C'_9)^\mu$ and $(C'_{10})^\mu$ that describe the $R_{K^{(*)}}$ anomaly. But we can assume a relatively larger value to eliminate the influence and it is not considered as a parameter.

Parameters and benchmark scenario

- Furthermore, assume

($\lambda_{232}, \lambda'_{233} = -\lambda'_{223} = -3\lambda'_{232}, m_{\tilde{b}_R} = m_{\tilde{b}_L}, m_{\tilde{\nu}_\tau}, m_{\tilde{\tau}_L} = 4\text{TeV}$) then we can plot the anomalies and constraints in the two-dimensional parameter space: ($\lambda'_{233}, m_{\tilde{b}_R}$) and ($\lambda_{232}, m_{\tilde{\nu}_\tau}$)

- $m_{\tilde{b}_R} = m_{\tilde{b}_L}$ for simplicity.
- $m_{\tilde{\tau}_L}$ has opposite contribution for $(g-2)_\mu$. The influence is not important as long as $m_{\tilde{\tau}_L} \gtrsim O(1\text{TeV})$. Here we choose 4 TeV.
- $\lambda'_{233} = -\lambda'_{223} \Leftarrow \lambda'_{233}, \lambda'_{223}$ and $m_{\tilde{b}_R}$ are the only parameters that influence $R_{D^{(*)}}$ and $R_{K^{(*)}}$ in our scenario. Assuming $\lambda'_{233} = \epsilon_1 \lambda'_{223}$, we found that $\epsilon_1 \sim (-3, -1)$ will give an overlap region of $R_{D^{(*)}}$ and $R_{K^{(*)}}$. When $|\epsilon_1|$ decrease, the coupling λ'_{233} of the overlap region will also decrease, so we choose $\epsilon_1 = -1$ here.
- $\lambda'_{233} = -\lambda'_{223} = -3\lambda'_{232} \Leftarrow \lambda'_{233}, \lambda'_{223}, \lambda'_{232}, m_{\tilde{b}_R}$ and $m_{\tilde{b}_L}$ are relevant for the constraints of $B \rightarrow K\nu\bar{\nu}$, $B_s - \bar{B}_s$ mixing and $D^0 \rightarrow \mu^+\mu^-$. Assuming $\lambda'_{233} \approx -\lambda'_{223} = \epsilon_2 \lambda'_{232}$, we found that $\epsilon_2 \sim (-6, -2)$, where $\epsilon_2 = -3$ gives the best fit.

Simulations

- Consider the processes $pp \rightarrow \bar{t}\mu^+\mu^-$ ($pp \rightarrow t\mu^+\mu^-$ is similar but with a larger background cross-section)
- Background:

Table 1: $pp \rightarrow \bar{t}\mu^+\mu^- X$ cross sections (fb)

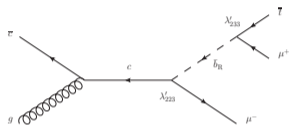
X	14 TeV	$M_{\mu^+\mu^-} > 0.15$ TeV	27 TeV	$M_{\mu^+\mu^-} > 0.15$ TeV	100 TeV	$M_{\mu^+\mu^-} > 0.15$ TeV
j	0.381	3.35×10^{-3}	1.06	1.05×10^{-2}	5.83	7.11×10^{-2}
b	4.23×10^{-3}	3.64×10^{-5}	9.47×10^{-3}	9.85×10^{-5}	3.84×10^{-2}	3.92×10^{-4}
$W^+ \rightarrow jj$	3.76×10^{-3}	2.75×10^{-5}	1.49×10^{-2}	1.33×10^{-4}	0.133	1.58×10^{-3}
$W^+ \rightarrow e^+\nu_e$	6.38×10^{-4}	5.68×10^{-6}	2.53×10^{-3}	2.68×10^{-5}	2.24×10^{-2}	2.28×10^{-4}
$W^+ \rightarrow \mu^+\nu_\mu$	6.15×10^{-3}	2.67×10^{-3}	2.64×10^{-2}	1.12×10^{-2}	0.242	0.120
$W^+ \rightarrow \tau^+\nu_\tau$	6.34×10^{-4}	6.09×10^{-6}	2.52×10^{-3}	3.08×10^{-5}	2.25×10^{-2}	2.81×10^{-4}
Total	0.396	6.10×10^{-3}	1.12	2.20×10^{-2}	6.29	0.194

$$^a p_T^{j,b,l} < 20 \text{ GeV}, E_T^{\text{miss}} < 20 \text{ GeV}$$

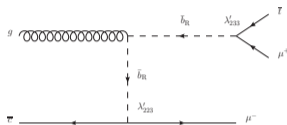
$$^b p_T^{t,\mu} > 20 \text{ GeV}, |\eta^{t,\mu}| < 2.5$$

Simulations

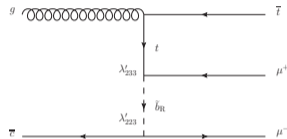
- Signal:



(a)



(b)

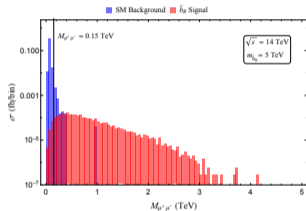


(c)

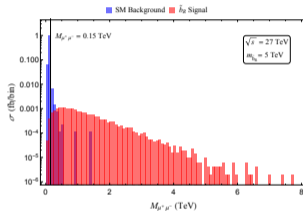
- Only λ'_{233} , λ'_{223} and $m_{\tilde{b}_R}$ contribute to the process $pp \rightarrow \bar{t}\mu^+\mu^-$. And what can be probed are actually these parameters, a projection of the scenario.
- Assume the luminosity $\mathcal{L} = 3000 \text{ fb}^{-1}$. $\sqrt{s} = 14 \text{ TeV}, 27 \text{ TeV}, 100 \text{ TeV}$.
- Signal significance $N = \frac{S}{\sqrt{S+B}}$.

Invariant mass distribution

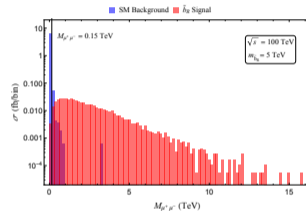
- Invariant mass $M_{\mu^+\mu^-}$ distributions at $\sqrt{s} = 14$ TeV, 27 TeV, 100 TeV



(d)



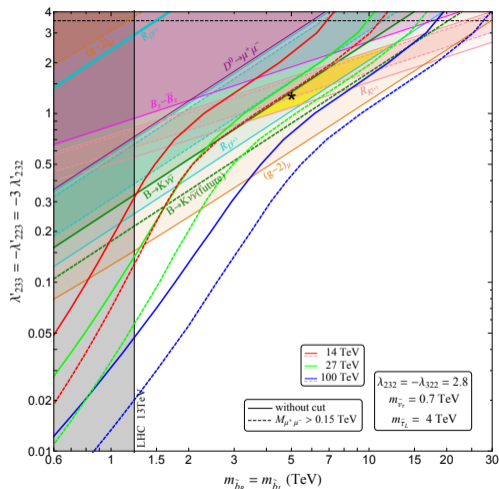
(e)



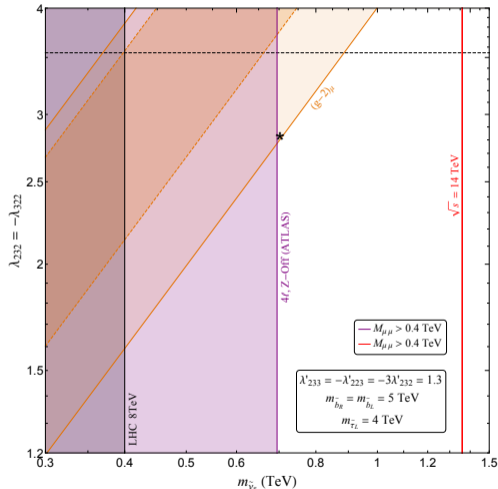
(f)

- We have used $\lambda'_{233} = -\lambda'_{223} = 1.3$, $m_{\tilde{b}_R} = 5$ TeV for the signal process.
- $p_T^{t,\mu} > 20$ GeV, $|\eta^{t,\mu}| < 2.5$, $\Delta R^{\mu\mu} > 0.4$ and $\Delta R^{t\mu} > 0.4$ for the minimal trigger cuts of $\bar{t}\mu^+\mu^-$

Anomalies and constraints in the parameter space



(g)



(h)

Anomalies and constraints in the parameter space

- The figure on the left corresponds to the black star in the figure on the right and vice versa.
- The invariant mass distributions are calculated at the value of black star in the figure on the left.
- Since many anomalies and constraints are independent of $(\lambda_{232}, m_{\tilde{\nu}_\tau})$, they become just numbers instead of curves in the figure on the right.

Anomaly/Constraint	Quantities in Figure(h)	Experimental value/limit
$R_{D^{(*)}}$	$\frac{R_{D^{(*)}}}{R_{D^{(*)}}^{\text{SM}}} = 1.05$	1.15 ± 0.04
$R_{K^{(*)}}$	$(C_9)^\mu = -(C_{10})^\mu = -0.23$	-0.35 ± 0.08
$D^0 \rightarrow \mu^+ \mu^-$	$\text{BR}(D^0 \rightarrow \mu^+ \mu^-) = 2.8 \times 10^{-10}$	$< 7.6 \times 10^{-9}$ (95% CL)
$B \rightarrow K^{(*)} \nu \bar{\nu}$	$R_{B \rightarrow K^{(*)} \nu \bar{\nu}} = \frac{\text{BR}(B \rightarrow K^{(*)} \nu \bar{\nu})}{\text{BR}_{\text{SM}}(B \rightarrow K^{(*)} \nu \bar{\nu})} = 4.6$	< 5.2 (95% CL)
$B_s - \bar{B}_s$ mixing	$\Delta M_{B_s} = (20.12 \pm 1.7) \text{ ps}^{-1}$	$(17.757 \pm 0.021) \text{ ps}^{-1}$

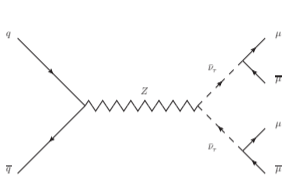
- The red, green and blue lines are the signal significance $N = 2$ curves at the center of mass energy $\sqrt{s} = 14$ TeV, 27 TeV and 100 TeV separately, before (solid lines) and after (dashed lines) applying the cut $M_{\mu^+\mu^-} > 0.15$ TeV.
- All the region above these curves corresponds to the signal significance $N > 2$. These curves bend downward because of the off-shell contribution of $pp \rightarrow \bar{t}\mu^+\mu^-$
- The yellow shaded region is the overlap of $(g-2)_\mu$, $R_{D^{(*)}}$ and $R_{K^{(*)}}$ favored region at 3σ level.
- This region is detectable when $\sqrt{s} > 27$ TeV at signal significance $N = 2$ level. It is the best scenario we can find for the detection purpose. Changing the value of $|\epsilon_1|$ could move the yellow shaded region to the upper left direction, but the detection curves will also move to the left faster than the yellow shaded region.
- We also put a future $B \rightarrow K^{(*)}\nu\bar{\nu}$ constraint line ($R_{B \rightarrow K^{(*)}\nu\bar{\nu}} = 1$) that can exclude the yellow shaded region.

Summary

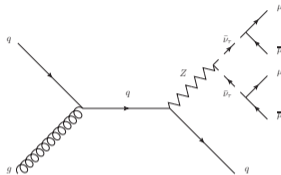
- $m_{\tilde{b}_R} \sim 3 - 12$ TeV ($|\lambda'_{233}| \sim 0.9 - 2.5$), $m_{\tilde{\nu}_\tau} \sim 0.7 - 0.9$ TeV ($|\lambda_{232}| \gtrsim 2.7$) \Rightarrow The first term in Eq(3) gives the main contribution of Δa_μ . The third term cannot be large due to the constraint of $B \rightarrow K^{(*)} \nu \bar{\nu}$ as one can see from Fig(g).
- The lower bound of $m_{\tilde{\nu}_\tau}$ comes from the 4-lepton search of ATLAS ([ATLAS-CONF-2021-011](#)). The 4-lepton signal in our scenario comes from the pair production of $\tilde{\nu}_\tau$ (+ jet) with $\tilde{\nu}_\tau \rightarrow \mu^+ \mu^-$, and we have also used the cut $M_{\mu\mu} > 0.4$ TeV.
- The red solid line in the figure on the right corresponds to the signal significance $N = 2$ when the $\sqrt{s} = 14$ TeV.
- Considering the 4-lepton signals, the whole $(g - 2)_\mu$ favored region is detectable ($R_{D^{(*)}}$ and $R_{K^{(*)}}$ are satisfied automatically since they are just numbers) at 14 TeV. This is a very distinctive and spectacular signal in our RPV3 scenario, although we cannot see much information about couplings.

Backup

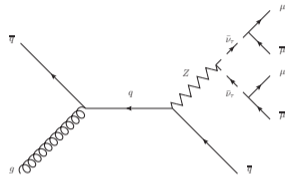
4-lepton signal



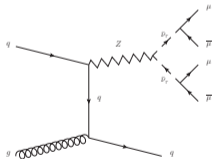
(i)



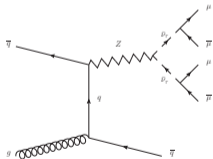
(j)



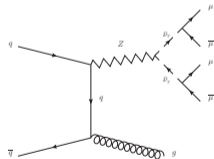
(k)



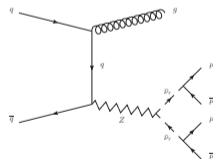
(l)



(m)



(n)



(o)

4-lepton signal

- We have used $M_{\mu\mu} > 400$ GeV, $p_{\text{T}}^{\mu} > 25$ GeV, $|\eta^{\mu}| < 2.47$, $p_{\text{T}}^j > 20$ GeV, $|\eta^j| < 2.5$, $\Delta R^{\mu\mu} > 0.4$ and $\Delta R^{j\mu} > 0.4$ same as the values mentioned in ATLAS-CONF-2021-011.
- $\sqrt{s} = 13$ TeV for the purple line and $\sqrt{s} = 14$ TeV for the red line in Figure(h).
- We have assumed the mass of the lightest neutralino is 100 GeV for the calculation of the branching ratio of $\tilde{\nu}_{\tau}$. But the $\text{BR}(\tilde{\nu}_{\tau} \rightarrow \mu\bar{\mu})$ is larger than 95% in our scenario when $|\lambda_{232}| > 1.2$